ResearchGate

See discussions, stats, and author profiles for this publication at: https://www.researchgate.net/publication/283511281

The Effects of Nanoparticle Morphology and Acyl Chain Length on Spontaneous Lipid Transfer Rates

ARTICLE *in* LANGMUIR · NOVEMBER 2015

Impact Factor: 4.46 · DOI: 10.1021/acs.langmuir.5b03291

READS

75

9 AUTHORS, INCLUDING:

Frederick Heberle

Oak Ridge National Laboratory

54 PUBLICATIONS **828** CITATIONS

SEE PROFILE

John Katsaras

Oak Ridge National Laboratory

250 PUBLICATIONS **4,837** CITATIONS

SEE PROFILE

Benxin Jing

Wayne State University

38 PUBLICATIONS **161** CITATIONS

SEE PROFILE

Mu-Ping Nieh

University of Connecticut

109 PUBLICATIONS **1,860** CITATIONS

SEE PROFILE

Available from: Ying Liu

Retrieved on: 04 April 2016

Langmuir

Article

pubs.acs.org/Langmuir

Effects of Nanoparticle Morphology and Acyl Chain Length on Spontaneous Lipid Transfer Rates

Yan Xia,[†] Ming Li,[‡] Kamil Charubin,[†] Ying Liu,[†] Frederick A. Heberle,[§,⊥] John Katsaras,[§,∥,⊥] Benxin Jing,[#] Yingxi Zhu,[#,○] and Mu-Ping Nieh*[,†,‡,▽]

[†]Department of Chemical and Biomolecular Engineering, University of Connecticut, Storrs, Connecticut 06269, United States

[‡]Polymer Program, Institute of Materials Science, University of Connecticut, Storrs, Connecticut 06269, United States

[§]Oak Ridge National Laboratory, Oak Ridge, Tennessee 37831 United States

[∥]Department of Physics and Astronomy, University of Tennessee, Knoxville, Tennessee 37996, United States

[⊥]Joint Institute for Neutron Sciences, Oak Ridge National Laboratory, Oak Ridge, Tennessee 37831, United States

[#]Department of Chemical and Biomolecular Engineering, University of Notre Dame, Notre Dame, Indiana 46556, United States

[▽]Department of Biomedical Engineering, University of Connecticut, Storrs, Connecticut 06269, United States

[○]Department of Chemical Engineering and Materials Science, Wayne State University, Detroit, Michigan 48202 United States

Supporting Information

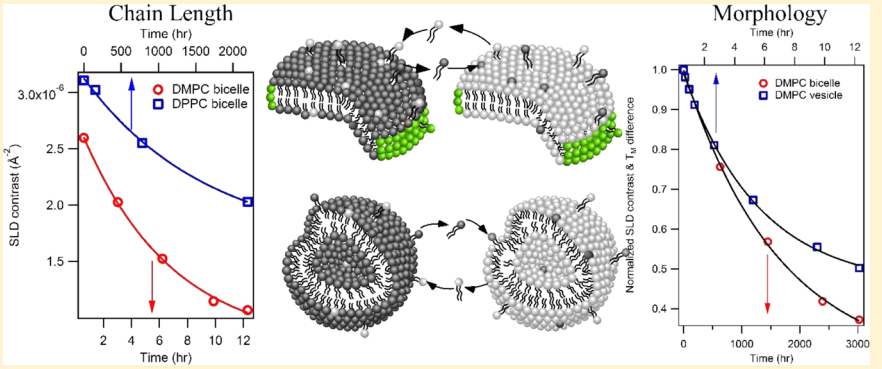

ABSTRACT: We report on studies of lipid transfer rates between different morphology nanoparticles and lipids with different length acyl chains. The lipid transfer rate of dimyristoylphosphatidylcholine (di-C_{14}, DMPC) in discoidal "bicelles" (0.156 h^{-1}) is 2 orders of magnitude greater than that of DMPC vesicles (ULVs) (1.1×10^{-3} h^{-1}). For both bicellar and ULV morphologies, increasing the acyl chain length by two carbons [going from di-C_{14} DMPC to di-C_{16}, dipalmitoylphosphatidylcholine (DPPC)] causes lipid transfer rates to decrease by more than 2 orders of magnitude. Results from small angle neutron scattering (SANS), differential scanning calorimetry (DSC), and fluorescence correlation spectroscopy (FCS) are in good agreement. The present studies highlight the importance of lipid dynamic processes taking place in different morphology biomimetic membranes.

INTRODUCTION

Molecular transfer between a host and its environment can affect the host's structural integrity and, ultimately, its function. In biology, for example, lipid transfer is ubiquitous in cell organelles.[1] Malfunction in the lipid transfer process can lead to cardiovascular[2] and autoimmune diseases,[3] atherosclerosis, Parkinson's disease,[4] cancer, obesity,[5] and diabetes,[6] to name a few. Lipid transfer can take place either through vesicular fusion or nonvesicular spontaneous transfer (involving individual lipids). The former mechanism plays an important role in protein transport of the exocytic and endocytic pathways, while the latter has been reported to play a significant role in intracellular lipid and protein transport.[7,8] Lipid transfer is usually associated with lipid transfer proteins (LTP), whereby individual lipids are "escorted" from one organelle to another. However, the detailed association and dissociation mechanisms of lipids with LTP are not fully understood.[1] It should be noted that lipid transfer can also take place in the absence of LTP, albeit at a slower rate.

To better understand lipid transfer between nanoparticles (NPs), it is necessary to accurately determine their lipid transfer rates. Here, we report lipid transfer rates in two lipid-based NP systems, namely, unilamellar vesicles (ULVs, also known as liposomes) and bilayered micelles (also known as bicelles) using different physical characterization techniques: these techniques can also be used to study molecular transfer rates of molecules

Received: September 1, 2015
Revised: October 25, 2015

© XXXX American Chemical Society

DOI: 10.1021/acs.langmuir.5b03291
Langmuir XXXX, XXX, XXX−XXX

other than lipids. ULVs are described by a core−shell structure, made up of a lipid bilayer shell and an aqueous core. An alternate morphology to the highly curved ULVs is flat bilayer fragments whose edges are stabilized either by α-helical apolipoproteins, such as nanodiscs,[9] or by short-chain lipids/surfactants/bile salt derivatives, in the case of bicelles (as shown in Figure 1a).[10,11]

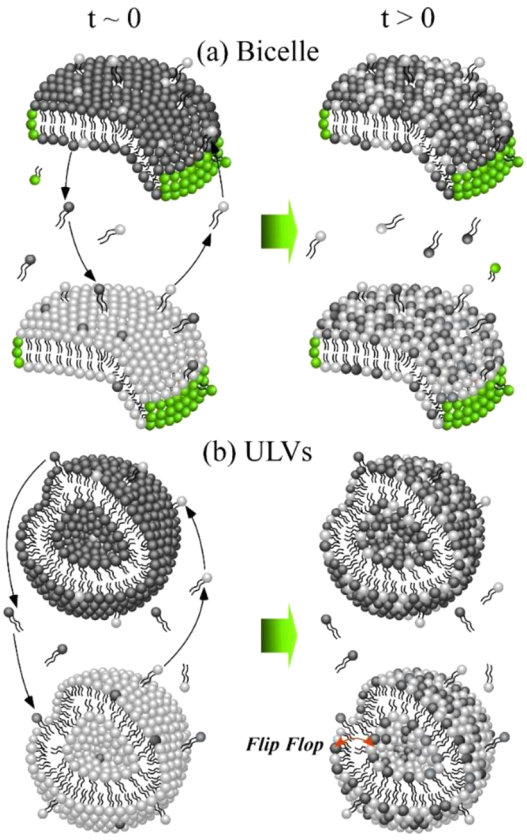

Figure 1. Schematic describing lipid transfer between (a) bicelles and (b) ULVs. The black and gray lipid headgroups indicate that the lipids are initially associated with different NPs. The green headgroups coating the bicelle rim represent short-chain lipids.

Over the years, much effort has been expended in developing ULVs and bicelles as biological membrane mimics, including understanding their structural[12,13] and mechanical[14] properties, and their lateral organization.[15,16] This understanding has led to knowledge of how lipids interact with membrane-associated proteins.[17,18] In addition, ULVs and bicelles have been used in biomedical applications[19,20] and as theranostic carriers.[21] Despite the fact that lipid-based NPs are extensively used in a number of scientific disciplines, an understanding of how their lipid dynamics are affected by their associated morphology is lacking. The two NP systems (i.e., ULV and bicelle) described here also happen to have narrow size distributions, allowing us to mitigate any effects that polydispersity may have on lipid transfer rates. Figure 1 shows how individual lipid molecules transfer between NPs. The different colored headgroups (black and gray) represent lipids that are virtually identical, but reside in different NPs at $t \sim 0$. Lipid exchange between NPs starts the moment the two populations are mixed, eventually reaching equilibrium, where NPs have a uniform distribution of black and gray lipids.

We have employed three methods including fluorescence correlation spectroscopy (FCS), small angle neutron scattering (SANS), and differential scanning calorimetry (DSC) to investigate the lipid transfer process. FCS can determine both lipid diffusion coefficient and fluorescent probe concentration in situ at the single-molecule level,[22,23] but it requires fluorescence-labeled probes which could alter the lipid's physical properties. To minimize this possibility, dipalmitoylphosphatidylcholine (DPPC) was labeled with BODIPY FL, a small hydrophobic fluorophore, that is attached to one of the lipid's acyl chains. On the other hand, to quantify lipid transfer rates using SANS and DSC, only isotope substitution is required (i.e., the use of deuterated lipid to replace protiated lipid). Separate deuterated NPs (d-NPs) and hydrogenated NPs (h-NPs) prepared in a contrast-match (CM) solvent (i.e., $\rho_s = x^*\rho_h + (1-x)^*\rho_d$, where ρ_s, ρ_h, ρ_d, and x are the neutron scattering length densities (NSLDs) for solvent, h-NP, d-NP, and the molar ratio of h-NP in an h/d-NP mixture, respectively) are "postmixed" in time-resolved SANS (TR-SANS). As molecular transfer proceeds, the SLDs of both types of NPs approach that of the contrast-matched (CM) solvent, leading to a decay of the scattered intensity, approaching the background as shown in Figure 2.[24−28] A similar

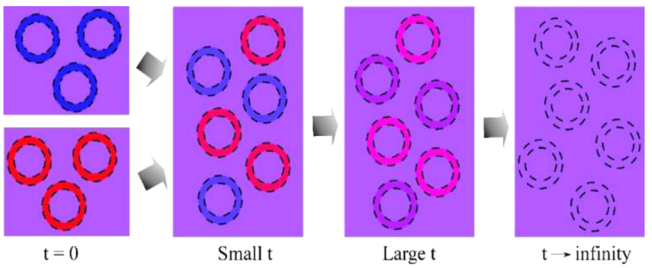

Figure 2. Schematic illustrating the contrast between NPs (blue and red) and the solvent (purple). Neutron contrast decays with time, due to the mixing of deuterated and protiated lipids.

approach can be used for time-resolved differential scanning calorimetry (TR-DSC), where the difference in main transition temperatures (ΔT_m) between d-NP and h-NP decreases as molecular transfer takes place.[29−32]

Lipid transfer rates obtained in this study show that they can differ by up to 2 orders of magnitude for different morphology (i.e., bicelles vs ULVs) NPs, or for same morphology NPs but with different length acyl chains (i.e., DMPC vs DPPC).

EXPERIMENTAL SECTION

NP Preparations. 1,2-Dipalmitoyl-*sn*-glycero-3-phosphocholine (h-DPPC), 1,2-dipalmitoyl-d62-*sn*-glycero-3-phosphocholine (d-DPPC), 1,2-dimyristoyl-*sn*-glycero-3-phosphocholine (h-DMPC), 1,2-dimyristoyl-d54-*sn*-glycero-3-phosphocholine (d-DMPC), 1,2-dipalmitoyl-*sn*-glycero-3-phospho-(1′-*rac*-glycerol) sodium salt (DPPG), 1,2-dimyristoyl-*sn*-glycero-3-phospho-(1′-*rac*-glycerol) sodium salt (DMPG), and 1,2-dihexanoyl-*sn*-glycero-3-phosphocholine (DHPC) were purchased from Avanti Polar Lipids (Alabaster, AL) and used without further purification. Deuterium oxide (D_2O, 99.9%) was purchased from Cambridge Isotope Laboratories, Inc. (Andover, MA).

Bicelles. Four different lipid mixtures, (1) h-DMPC/DMPG/DHPC, (2) d-DMPC/DMPG/DHPC, (3) h-DPPC/DPPG/DHPC, and (4) d-DPPC/DPPG/DHPC with a molar ratio Q [total long-chain to short-chain ratio, i.e., ([DMPC] + [DMPG])/[DHPC])] = 3, and R [(long-chain lipid charge ratio, i.e. [DMPG]/([DMPG] + [DMPC])] = 0.05, were prepared. The dry lipid powders were codissolved in chloroform, and the chloroform was then removed under a stream of nitrogen. The lipid films were then placed overnight under vacuum to remove any residual chloroform. The dry lipid films were subsequently hydrated using the appropriate CM solvents for SANS experiments (the detailed formulas for the CM solvents are shown in the Supporting Information

DOI: 10.1021/acs.langmuir.5b03291
Langmuir XXXX, XXX, XXX−XXX

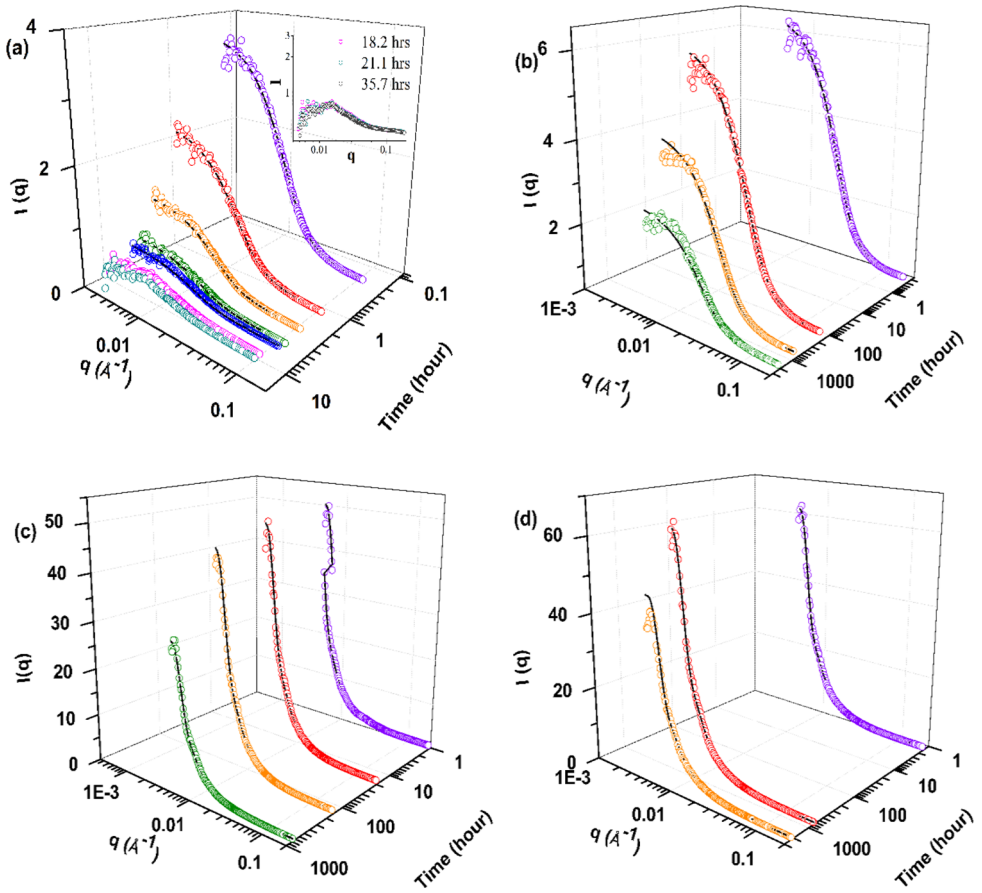

Figure 3. Evolution of SANS patterns (I vs q) from bicelles (a and b) and ULVs (c and d) composed of (a) h-DMPC/DMPG/DHPC and d-DMPC/DMPG/DHPC, (b) h-DPPC/DPPG/DHPC and d-DPPC/DPPG/DHPC, (c) h-DMPC/DMPG and d-DMPC/DMPG, and (d) h-DPPC/DPPG and d-DPPC/DPPG in CM water at 10 °C. The inset in (a) shows the invariant SANS data for d- and h-DMPC/DHPC/DMPG bicelle mixture after 18 h, indicating that the lipid transfer almost reaches equilibrium.

Table S1), or deionized water for FCS experiments, to a lipid concentration of 10 wt %. Samples were then temperature cycled between 4 and 50 °C until they were liquid-like and transparent at a temperature lower than T_M (i.e., 4 °C), and viscous at higher than T_M (i.e., 50 °C), features associated with the presence of bicelles. The bulk bicelle solutions were diluted to 1 wt % using corresponding CM solvents, or deionized water for the lipid transfer experiments, and were stored at 10 °C prior to experimentation. The temperature was chosen on the basis of the long stability of DMPC bicelles (on the order of days) since higher temperature may cause bicelles to coalesce,[33−36] resulting in misinterpretation of the data.

Unilamellar Vesicles (ULVs). Four different lipid mixtures were prepared, namely, (5) h-DMPC/DMPG, (6) d-DMPC/DMPG, (7) h-DPPC/DPPG, and (8) d-DPPC/DPPG, with a charge ratio R = 0.05. Dry lipid powders were dissolved in chloroform, and the chloroform was removed under a stream of nitrogen while the sample was slightly above ambient temperature. Residual chloroform was removed by placing the dry samples under vacuum overnight. The lipid films were then hydrated to a lipid concentration of 1 wt % using appropriate CM solvents for SANS experiments. A solution of 0.01 wt % sodium azide was added to DSC samples in order to prevent biodegradation. Samples were then exposed to several freeze-thaw cycles and vigorous vortexing. ULVs were produced by extruding (31 passes through the filter) the lipid solutions through 100 nm polycarbonate membranes (Avanti Polar Lipids, Alabaster, AL). ULV solutions at a lipid concentration of 1 wt % were stored at 10 °C prior to experimentation. The temperature was chosen to be the same as that of bicelles for comparison purpose.

Small Angle Neutron Scattering (SANS). SANS experiments were carried out at the EQ-SANS instrument, which is located at the Oak Ridge National Laboratory (ORNL, Tennessee) Spallation Neutron Source (SNS). A sample-to-detector distance of 4 m and a 30 Hz "frame-skipping" mode were used, resulting in two wavelength (λ) bands with maxima at 2.5 and 9.4 Å yielding scattering vectors, q [$q = 4\pi/\lambda \sin(\theta/2)$, where θ is the scattering angle] ranging from 0.005 to 0.25 Å^{-1}. Equal molar h-NP and d-NP (either bicelle or ULV) mixtures were loaded into 1 mm path-length quartz banjo cells (Hellma USA, Plainview, NY) and mounted in a temperature-controlled cell holder at 10 °C. 2D SANS data were collected at different mixing times and reduced to 1D scattering patterns using the ORNL Mantid program (http://www.mantidproject.org/). Data were corrected for detector pixel sensitivity, dark current, and sample transmission. A discoidal model with polydisperse radius and a spherical shell model with polydisperse radius were used to fit the bicelle and vesicle SANS data, respectively, in order to obtain the NSLD contrast and dimensions of the NPs. The incoherent background was not subtracted from the corrected SANS data, but was used as a fitting parameter in the SANS models.

Differential Scanning Calorimetry (DSC). Equimolar amounts of deuterated (d-DMPC/DMPG) and protiated (h-DMPC/DMPG) ULVs were mixed under gentle vortexing. The stock solution was incubated at 10 °C and stored in a thermostated water bath. For the different mixing times, aliquots were taken from the stock solution and measured using a TA Nano differential scanning calorimeter (New Castle, DE). A ULV solution (0.3 mL), and its corresponding solvent, were loaded into the sample and reference cells, respectively. Experiments were conducted under 3 atm of pressure, and sample and solvent were equilibrated at 5 °C for 10 min prior to experimentation. The final scans ranged in temperature from 5 to 40 °C and were collected at a scan rate of 0.5 °C/min. The same experimental protocol was used to collect the background scans, where

DOI: 10.1021/acs.langmuir.5b03291
Langmuir XXXX, XXX, XXX−XXX

both sample and reference cells contained solvent, but no ULVs. The generated DSC profiles were corrected for solvent background and baselines using TA's proprietary software.

Fluorescence Correlation Spectroscopy (FCS). Lipid transfer rates between DMPC bicelles were determined by FCS at 10 °C. Temperature was controlled by a thermal stage (INSTEC HCS60), which was mounted on an inverted microscope (Zeiss Axio A1) equipped with a 100× objective lens (NA = 1.4, oil immersion).[37] Briefly, an argon laser (Melles Griot, λ_{ex} = 488 nm) was focused on the bulk bicelle solution and the fluorescence photon count was detected by two single-photon-counting modules (Hamamatsu). The emission fluorescence intensity, $I(t)$, of the fluorescent lipid β-BODIPY FL C5-HPC (2-(4,4-difluoro-5,7-dimethyl-4-bora-3*a*,4*a*-diaza-*s*-indacene-3-pentanoyl)-1-hexadecanoyl-*sn*-glycero-3-phosphocholine) (Invitrogen) in DMPC bicelles was measured using a small laser focal volume to obtain the autocorrelation function,[22,23] as expressed below:

$$G(\tau) = \frac{\langle \delta I(t)\delta I(t+\tau)\rangle}{\langle I(t)\rangle^2} \quad (1)$$

Here $\delta I(t) = I(t) - I(t)$, and $I(t)$ and $I(t+\tau)$ are the fluorescence intensity at time t and $(t+\tau)$, respectively. The laser focal volume was calibrated at ω_{xy} = 263 nm for the radial radius, and ω_z = 5.85 μm for the axial radius using the Alexa Flour 488 (Invitrogen), which has a known diffusion coefficient D = 435 $\mu m^2/s$ at 22.5 °C when in a dilute aqueous solution.[38]

RESULTS

ULVs are known to be stable over extended periods of time (months). However, weakly or noncharged spontaneously forming bicelles may coalesce with each other, forming larger-sized bicelles,[33] ULVs,[34] or even multilamellar vesicles.[35,36] It is also known that increasing charge density and retaining long-chain lipid at low-T gel phase can inhibit bicelles from coalescing with each other.[33,39] Since the aim of the current study is to investigate transfer rates of *individual* lipid molecules, bicelle coalescence was kept to a minimum through the addition of 5 mol % of a long-chain, charged lipid (i.e., [charged long-chain]/[total long-chain] = 5 mol %). Figure 3a,b show time-resolved SANS curves of h-DMPC bicelles after mixing with d-DMPC bicelles (h-/d-DMPC bicelles) and h-/d-DPPC bicelles, respectively. The fact that the scattering patterns for the h-/d-DPPC bicelles (Figure 3b), and individual h-DMPC and d-DMPC bicelles (Supporting Information Figure S1) do not change with time shows that bicelles are structurally stable (i.e., minimal or no coalescence). Moreover, the best fits to the h- and d-ULVs result in similar radii, as do the h- and d-bicelles, indicative of a minimal isotope effect (Supporting Information). Noteworthy findings from these data are the following: (a) As predicted, the decrease in SANS intensity with time indicates that the protiated and deuterated lipids from different bicelles are exchanging with each other; and (b) SANS curves of mixed bicelles show the presence of little or no structure factor arising from interparticle interactions, unlike those from pure h- or d-bicelle solutions (Supporting Information Figure S1). This is expected as the bicelle NSLD is matched to that of the solvent.[40] The SANS data are therefore fitted using a single form factor, $P(q)$ (the particle's shape as described in Supporting Information), without the need of a structure factor. The solid curves in Figure 3a,b are best fits to the data using a discoidal model,[41] with contrast being the only variable (the best fitted contrast obtained from the SANS data are shown in Supporting Information Tables S2 and S3). Fits of the data show that the average radius and thickness of DMPC and DPPC bicelles are approximately 66 and 29 Å, and 69 and 34 Å, respectively. Bicelle bilayer thicknesses are found to be similar to those of a typical gel phase lipid bilayer (i.e., 30 and 34 Å for DMPC[42] and DPPC,[43] respectively). The "apparent" bicelle thickness is the result of neutron contrast, which, in this case, is most sensitive to the contrast between the solvent and the lipid acyl chains: the association of CM water with the protiated lipid head groups makes the head groups practically invisible to neutrons.[44] As exchange proceeds, contrast between the bicelles and solvent decreases, resulting in a reduced scattered intensity [e.g., the SANS data at t > 10 h postmixing of h-/d-DMPC bicelles in Figure 3a). However, complete elimination of coherent scattering cannot be achieved since h-DHPC segregated from the h- and d-DMPC mixture, resulting in a certain amount of residual scattering (possibly the structure factor), as shown in the inset of Figure 3a. However, the near invariance of SANS intensity after 18 h suggests that the lipid transfer almost reaches equilibrium. It should be noted that the residual scattering intensity was weak and did not affect analysis of the early stage lipid transfer data.

Lipid transfer rates can then be determined from the best-fit, $\Delta\rho$ under the following assumptions: (a) a pseudo-steady state; (b) a single mechanism for lipid transfer; and (c) symmetric lipid transfer, in which case $\Delta\rho = |\rho_{CM} - \rho_{h\text{-}NP}| = |\rho_{d\text{-}NP} - \rho_{CM}|$. Assumption (a) is valid as there is no lipid accumulation in the water phase or in NPs. Assumption (b) can be applied when there is no other competing exchange process in the system. Assumption (c) lies in the minimum isotope effect. As a result, $\Delta\rho$ is described by a single exponential time decay (detailed derivation is given in the Supporting Information). Furthermore, in the case of bicelles, only interparticle lipid transfer is considered, resulting in the following expression for the lipid transfer rate:

$$|\Delta\rho| = |\Delta\rho_0| e^{-k_{Bic}t} \quad (2)$$

Here, $|\Delta\rho_o|$ and k_{Bic} are the initial $|\Delta\rho|$ (i.e., t = 0) and the interparticle lipid transfer rates between bicelles, respectively. In the following discussion, $k_{Bic,DMPC}$ and $k_{Bic,DPPC}$ are used to represent the transfer rate constants of DMPC and DPPC bicelles, respectively. Figure 4 shows the best fits for the contrast decay data from DMPC and DPPC bicelles, where $k_{Bic,DMPC}$ (0.156 ± 0.011 h^{-1}) is 550 times greater than $k_{Bic,DPPC}$ ($2.81 \times 10^{-4} \pm 2.0 \times 10^{-5}$ h^{-1}). The slower molecular transfer observed for the longer-chain DPPC lipid is most likely due to the lower

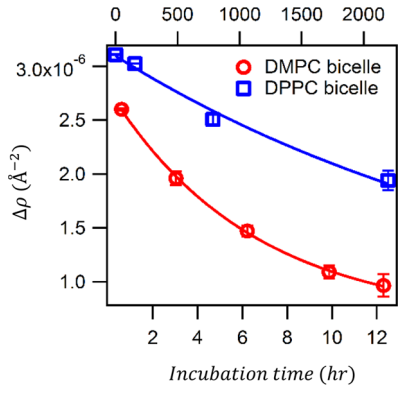

Figure 4. NSLD contrast as a function of time after h and d bicelles were mixed at 10 °C. The top and bottom X-axes are for DPPC/DPPG/DHPC and DMPC/DMPG/DHPC bicelles, respectively. Solid lines are the single exponential decay fits to the data, where R^2 for DMPC and DPPC bicelles are 0.999 and 0.985, respectively.

DOI: 10.1021/acs.langmuir.5b03291
Langmuir XXXX, XXX, XXX−XXX

critical micellar concentration, CMC (6.0 and 0.46 nM for DMPC and DPPC, respectively), and the lipid's higher T_M (24 and 41 °C for DMPC and DPPC, respectively). A lower CMC inhibits lipid exchange between bicelles and solution, while the higher-T_M lipid (i.e., DPPC) resides deeper in the gel phase (i.e., a more rigid bilayer) for a given T, most likely leading to a higher energy barrier impeding individual lipid molecules from dissociating from the bilayer.

Figure 3c,d shows SANS curves of h-/d-DMPC/DMPG and h-/d-DPPC/DPPG ULVs, respectively. The scattering patterns for these systems are different. Oscillations along the SANS curves are good indicators of low size polydispersity, and peak locations correspond to particle size. It should be noted that the absence of a multilamellar peak at ~0.1 $Å^{-1}$ implies that the multipass extrusion and high bilayer charge density have successfully eliminated most of the naturally forming multilamellar vesicles. The data are best fit using a polydisperse spherical core−shell model of fixed shell thickness (Supporting Information Tables S4 and S5). The observed intensity decay rates are significantly slower than those obtained from corresponding bicellar lipid mixtures. In fact, there is slight decrease in the SANS intensity over the first 150 h, indicating a much slower lipid transfer rate compared to that of bicelles. The SANS intensity from DMPC/DMPG decreased by approximately 30% after 30 days. However, we are unable to accurately determine lipid transfer rates for ULVs using SANS due to the limited number of data sets. Because of this, lipid transfer rates for DMPC/DMPG ULVs were determined by DSC. Nevertheless, the contrast obtained from these four data points followed an exponential decay as a function of time, consistent with the theoretical prediction. Regarding DPPC/DPPG ULVs, the SANS intensity dropped by 30% after 90 days (~2160 h). However, this drop was possibly caused by the degradation of DPPC instead of lipid transfer since the three data points (i.e., day 1, day 30, and day 90) did not follow a reasonable exponential decay. Therefore, the data point obtained on day 90 was not used.

The DSC endotherms of h-/d-DMPC/DMPG ULV mixtures as a function of time contain two peaks: one corresponding to the lower T_M of d-rich (T_d) and another representing the higher T_M of h-rich NPs (T_h) (Figure 5). As a function of time, h- and d-NPs exchange lipids, causing the peaks associated with d-rich and h-rich ULVs to move toward each other, until the two peaks merge into one when lipid exchange is complete (Supporting Information Figure S4). To a first-order approximation, T_M is linearly dependent on lipid composition,[55] i.e., $T_M = T_{d,0}\phi_d + T_{h,0}\phi_h$, where $T_{d,0}$ and $T_{h,0}$ are the initial T_M of d-DMPC and h-DMPC ULVs, respectively.

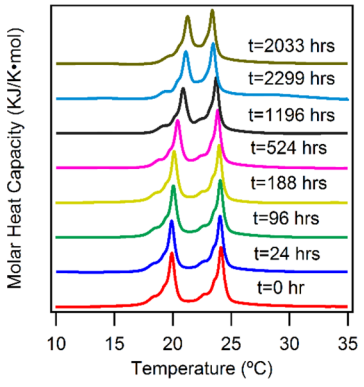

Figure 5. DSC scans of h-/d-DMPC/DMPG ULV at different incubation times. Scans are vertically displaced for better viewing.

Figure 6 illustrates $\Delta T_M = T_h - T_d$ of h-/d-DMPC ULVs as a function of time after mixing. For comparison purposes, the $\Delta\rho$ obtained from the time-resolved SANS data (Figure 3c) is also presented. Their normalized values, namely, $(\Delta T_M/\Delta T_{M,0})$ and $(|\Delta\rho|/|\Delta\rho_0|)$ as a function of incubation time are shown in the inset to Figure 6, where $\Delta T_{M,0}$ represents ΔT_M at $t = 0$. The fact that the results obtained from these two different techniques are in such good agreement lends validity to the experimental techniques used to study lipid transfer rates in ULVs. However, unlike bicelles where lipid transfer only takes place between particles, in ULVs one must also account for lipid flip-flop between the inner and outer bilayer leaflets using the following analysis (as shown in the Supporting Information)

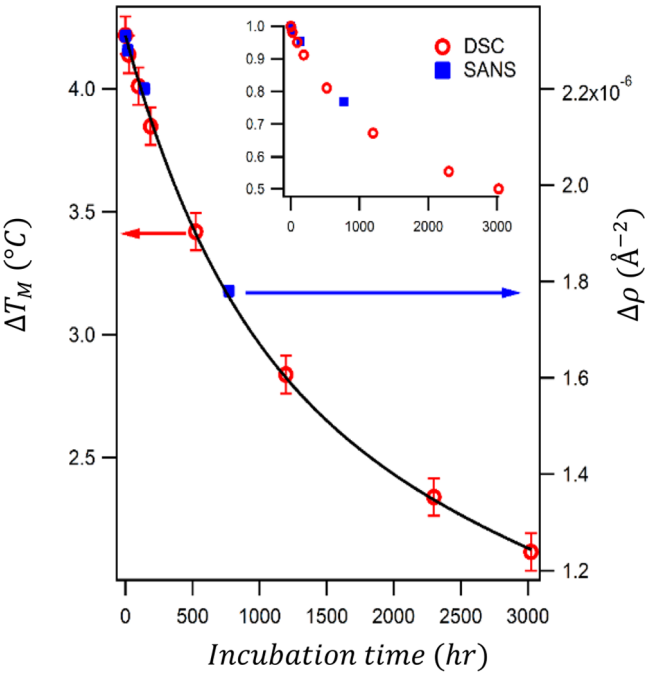

Figure 6. ΔT_M (red ○, left axis) and $\Delta\rho$ (blue ■, right axis) of h-/d-DMPC/DMPG ULVs as a function of mixing time. The solid line is the best fit to the data using eq 3, resulting in $R^2 = 0.999$. The inset shows the normalized values of $\Delta T_M/\Delta T_{M,0}$ and $|\Delta\rho|/|\Delta\rho_0|$ as a function of time. It is clear that the data from the two techniques are in very good agreement.

$$\Delta T_M = \Delta T_{M,0}\left[\frac{2k_{FF} + k_{inter} + \sqrt{4k_{FF}^2 + k_{int\ er}^2} - 2ak_{inter}}{2\sqrt{4k_{FF}^2 + k_{int\ er}^2}}\right]e^{\lambda_1 t} - \Delta T_{M,0}\left[\frac{2k_{FF} + k_{inter} - \sqrt{4k_{FF}^2 + k_{int\ er}^2} - 2ak_{inter}}{2\sqrt{4k_{FF}^2 + k_{int\ er}^2}}\right]e^{\lambda_2 t} \quad (3)$$

$$\lambda_{1,2} = \frac{-(k_{inter} + 2k_{FF}) \pm \sqrt{k_{int\ er}^2 + 4k_{FF}^2}}{2} \quad (4)$$

where k_{FF}, k_{inter}, and a are the transmembrane flip-flop rate constant, the lipid interparticle transfer rate constant between bilayer leaflets, and the ratio of inner leaflet lipids to the total

DOI: 10.1021/acs.langmuir.5b03291
Langmuir XXXX, XXX, XXX−XXX

number of lipids in one ULV, respectively. It should be noted that both k_{FF} and k_{inter} are (so is k_{Bic}) independent of concentration, as previously reported.[26,45] Equations 3 and 4 can be applied to the analysis of SANS data simply by replacing ΔT_M and $\Delta T_{M,0}$ with $|\Delta\rho|$ and $|\Delta\rho_0|$, respectively. The best fits to the data yield values for k_{FF} and k_{inter} [obtained from eqs 3 and 4] of $1.01 \times 10^{-3} \pm 6.54 \times 10^{-5}$ and $8.75 \times 10^{-5} \pm 2.8 \times 10^{-5}$ h^{-1}, respectively (Table 1). The obtained k_{inter} agrees well with literature values ($\sim 1 \times 10^{-3}$ h^{-1}) for DMPC ULVs at 10 °C.[46,47] However, the DPPC transfer rate in ULVs is not accessible due to its very slow kinetics, as was mentioned previously. We can only estimate the upper limit of k_{inter} is 10^{-5} h^{-1} based on a 2% change in $|\Delta\rho|$ over 770 h. A similar expression was derived to describe ULV lipid transfer using a different approach.[24] Of note is that the interparticle transfer rate between ULVs is significantly lower than what we observed in bicelles, even after correcting for lipid flip-flop. The enhanced lipid transfer rate, in the case of bicelles, is most likely due to the presence of the detergent-like, short-chain lipid DHPC. The fact that the half-life of lipid flip-flop (associated with the k_{FF}) can range anywhere from hours to months, depending on lipid composition, temperature, etc., was determined through DSC and SANS measurements.[48,49]

Table 1. Lipid Transfer Rates for Bicelles and ULVs Measured by SANS, DSC, and FCS

	interparticle transfer rate (h^{-1})	flip-flip rate (h^{-1})
DMPC bicelle	0.156 ± 0.011 (SANS) 0.210 ± 0.008 (FCS)	N/A
DPPC bicelle	$(2.81 \pm 0.20) \times 10^{-4}$ (SANS)	N/A
DMPC vesicle	$(1.01 \pm 0.06) \times 10^{-3}$ (DSC)	$(8.75 \pm 2.8) \times 10^{-5}$ (DSC)
DPPC vesicle	$<10^{-5}$	N/A

For additional validation, the lipid transfer rate between bicelles was also determined by FCS. In contrast to SANS and DSC experiments, FCS requires a probe molecule to measure lipid transfer, in our case the fluorescent lipid β-BODIPY FL C5-HPC. Bicelles, each on average containing two BODIPY FL–lipid probes (with the BODIPY FL–lipid concentration of 11.4 nM in the bicelle concentration of 7.2 nM before lipid exchange), were prepared and mixed with the same concentration of unlabeled bicelles. Figure 7a shows the time evolution of the autocorrelation function, $G(\tau)$, of mixed samples which shifts to lower values as a function of time. $G(\tau)$ is fitted using the three-dimensional Gaussian equation – eq 5,[22] yielding the diffusion coefficient D, which remained the same throughout the lipid transfer measurement, ruling out bicelle coalescence and possible effects due to the concentration $[c]$ of fluorescent bicelles. $G(\tau)$ is expressed as follows:

$$G(\tau) = ([c]\pi^{1.5}\omega_z\omega_{xy}^2)^{-1}\left(1 + \frac{4D\tau}{\omega_{xy}^2}\right)^{-1}\left(1 + \frac{4D\tau}{\omega_z^2}\right)^{-0.5} \quad (5)$$

Here, ω_z and ω_{xy} are the axial and radial radii of the laser focal volume, respectively. A decrease in $G(0)$ indicates an increase in $[c]$ (also shown in Figure 7b), supporting the notion of lipid transfer taking place between bicelles. Since the diffusion coefficient of the bicelles (~ 18 $\mu m^2/s$) in solution is much larger than the lateral diffusion coefficient of gel phase DMPC, they are completely decoupled from each other. More importantly, since $[c]$ shows the same time dependence as $|\phi_h - \phi_d|$, the lipid transfer rate is determined by fitting the $[c]$ profile (Figure 7b) using

$$[c](t) = [c_0](2 - e^{-k_{Bic}t}) \quad (6)$$

where $[c_0]$ is $[c]$ at $t = 0$. Figure 7b yields $k_{Bic,DMPC}$ (0.210 ± 0.008 h^{-1}) for DMPC bicelles, a value greater than what was determined from SANS measurements presumably owing to the different chemical structure of the fluorescence probe from that of the native lipid. However, compared to DSC and SANS, FCS is a better technique for studying a system with high transfer rates (i.e., >1 h^{-1}).

DISCUSSION

All three experimental techniques produced results that were in good overall agreement with each other. The fact that the transfer rate decreases by 2 orders of magnitude as the acyl chains become longer by two carbons (i.e., from DMPC to DPPC) indicates a strong correlation between lipid transfer rates and lipid acyl chain length. The acyl chain length has been found to profoundly affect the spontaneous transfer kinetics in vesicular systems, and has been rationalized as the energy required for a single lipid molecule to extricate itself from a bilayer.[50−52] The free energy of the lipid transfer with low aqueous solubility,[53] namely, from a micelle to the water phase, can be estimated by the critical micellar concentration (CMC) by $\Delta G^t = -RT \ln(CMC/55.5)$,[54] where $(CMC/55.5)$ is the molar ratio of lipid in the water phase,

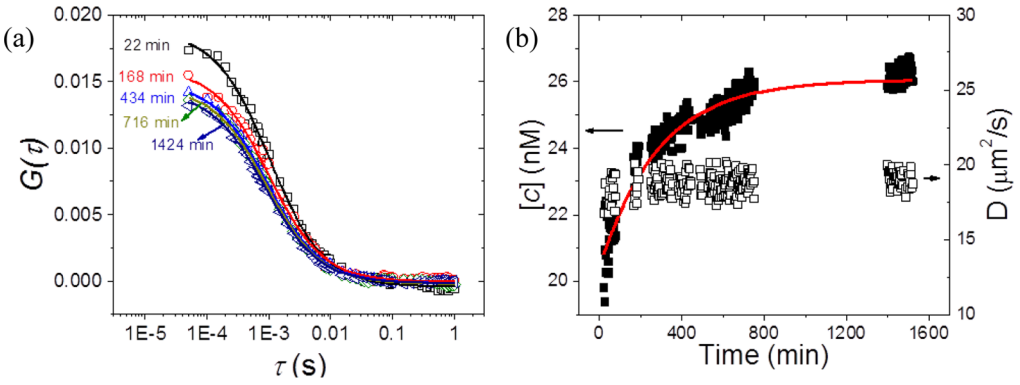

Figure 7. (a) Time-dependent autocorrelation function, $G(\tau)$, and fits (solid lines) to the data using eq 5. (b) Concentration $[c]$ (left Y-coordinate axis) and diffusion coefficient D (right Y-coordinate axis) of fluorescence labeled DMPC/DMPG/DHPC bicelles as a function of time. The solid red line is the fit to the data using a single exponential decay with $R^2 = 0.922$.

DOI: 10.1021/acs.langmuir.5b03291
Langmuir XXXX, XXX, XXX−XXX

resulting in a ΔG^t of 54 and 60 kJ/mol for DMPC (CMC: 6 nM)[55] and DPPC (CMC: 0.46 nM),[56] respectively. This shows that lipids with faster transfer rates are more water-soluble. Ferrell et al. found that the dissociation rate of a PC lipid (in the range from C_{12} to C_{16}) at 37 °C is $^1/_9$ of the original through the addition of just one carbon to each acyl chain.[50] On this basis, DMPC transfer rates should be ∼80 times faster than those of DPPC. However, in the current study a more significant impact of acyl chain length on lipid transfer was observed when both DMPC and DPPC are in the gel phase. Namely, in ULVs and bicelles DPPC transfers ∼100 and ∼600 times slower, respectively, than DMPC in the same morphology NPs.

In the L_α (liquid disordered) phase, Ferrell et al. have found that $\Delta G^‡ - \Delta G^t$ is around 40 (kJ/mol),[57,58] where $\Delta G^‡$ represents the Gibbs energy of the transition activation complex, which presumably forms on the bilayer surface. To estimate $\Delta G^‡$, we substitute the obtained rate constants from DMPC and DPPC (Table 1) into the Eyring–Polanyi equation $k = (k_B T/h)e^{-\Delta G^‡/RT}$, where k_B is the Boltzmann constant and h is Planck's constant. $\Delta G^‡$ is then estimated to be ∼93 and 107 kJ/mol for DMPC and DPPC, respectively, indicating a larger energy gap between $\Delta G^‡$ and ΔG^t for lipid gel phase ($\Delta G^‡ - \Delta G^t$ is 39 and 47 kJ/mol for DMPC and DPPC, respectively). This analysis suggests that the transition state complex strongly depends on the lipid phase. For example, several cavity models have been proposed in which a suitable size cavity is formed to explain the partition of lipids between nonpolar and aqueous phases at the transition state.[52,59] Moreover, the fact that a van der Waals interaction among acyl chains in the lipid gel phase is stronger than that in the liquid crystalline phase explains that the difference in lipid transfer rate upon increasing acyl chain length would be larger in the gel phase. Therefore, more energy is presumably required for extracting longer acyl chain lipids from the bilayer.

In bicelles, the lipid transfer rates for DMPC and DPPC are ∼150 and >30 times faster, respectively, than those in the corresponding ULVs. In the case of ULVs, the slow transmembrane lipid flip-flop is presumably the primary factor affecting lipid transfer, since lipids in the inner bilayer leaflets of ULVs have to flip to the outer leaflet in order to exchange with lipids in the bulk water phase. However, flip-flop may not be the only factor that affects lipid transfer rates; otherwise, an initial transfer rate similar to what was observed in bicelles should have been seen during the initial exchange between lipids in the outer bilayer leaflets of ULVs and bulk water (at least 50% or more). A much lower value of k_{inter}, compared to k_{Bic}, implies that the transfer rate also depends on NP morphology. A SANS study has reported that the lipid transfer rate of DMPC in lipoprotein nanodiscs (instead of bicellar discs) is 20 times greater than that of DMPC in fluid phase vesicles (27 °C).[26] The proposed mechanism for the enhanced transfer rate was attributed to the lower entropy that arises from the closer packing of lipids induced by the lateral compression from the lipoprotein "belt". However, this rationale is not applicable to bicelles whose rims are stabilized by the short-chain DHPC, and which *spontaneously form* the discoidal structure. It has been shown that the line tension at the rim (analogous to the concept of the lateral compression) would lead to disc fusion, as was previously reported,[33] requiring less energy to drive the long-chain lipids into the water phase. A possible scenario is that the enhanced lipid transfer rate is mainly the result of long-chain lipids which reside at the interface region between the DHPC and the long-chain enriched domains, diffusing faster than the bulk gel lipids. This may also explain the larger effect that increased acyl chain lipids have on bicelles compared to that of ULVs. Another possible (but unlikely) scenario is that the short-chain DHPC, which has a higher solubility (CMC = 15 mM), might serve as a transport carrier to "escort" more hydrophobic DMPC and DPPC from one particle to another, possibly resulting in the enhanced lipid transfer rates for the long-chain lipids. However, the 600-fold increase of the lipid transfer rate from DPPC to DMPC does not seem to support DHPC-mediated transfer; otherwise, similar transfer rates would be expected. A fluorescence study on DMPC/DHPC bicelle (15 wt %) suggests that fusion of the bicelles enhances the lipid transfer at temperatures from 17 to 35 °C.[60] This could also be one of the reasons for the fast lipid transfer in bicelles compared to that in ULVs. Since bicelles in this study did not change their dimension throughout the experiment (S1 in Supporting Information), if fusion was responsible for the fast transfer rate, the process would have involved dissociation of the larger bicelles. Though this possibility cannot be completely excluded, it is highly unlikely for the following reasons. First, such constant "fusion/dissociation" among bicelles is not consistent with the significant difference in the lipid transfer rates between DPPC and DMPC bicelles at the same lipid concentration, where the fusion rates are expected to be similar for both. It should be noted that the experimental condition in ref 60 was different from that in the current study in terms of temperatures (>17 °C), lipid concentration (15 wt %), and composition (in the absence of charged lipid). The addition of 5 mol % charged lipids (DMPG or DPPG) could further lower the fusion frequency as reported in a recent study of diffusion-limited bicelle coalescence in a charged bicelle system.[33] A molecular simulation and lipid transfer rate measurements as a function of DHPC concentration will be performed in the future to further our understanding in this regard.

In addition to the aforementioned changes in lipid transfer rates, the advantages and limitations of each technique are summarized in Table S6 of the Supporting Information, thus enabling researchers to select the appropriate physical characterization technique. It should also be noted that these techniques are not limited to lipids, but may also be used to study other systems, such as polymers.[25,27]

CONCLUSIONS

Knowledge of molecular transfer rates provides important insights into the thermodynamic stability of different nanomorphologies and their possible biological implications. The current study has clearly shown that both lipid acyl chain length and NP morphology affect lipid transfer rates. Specifically, lipids with longer acyl chains have lower transfer rates because of their lower solubility in water, compared to their shorter-chain counterparts. We have also found that, for a given lipid, the transfer between bicelles can be two orders of magnitude faster than that between ULVs. The morphological dependence of lipid transfer rate is presumably associated with the enhanced rate occurring at the intermediate domain between the liquid disordered (L_α) and gel phases that exist within the bilayer. Good agreement between the three techniques (SANS, DSC, and FCS) used in this study is also a good indicator of their complementarity. Molecular simulations may further advance our understanding of the molecular and atomic mechanisms involved in lipid transfer. The current data imply that lipid transfer rates for a given lipid may differ drastically in living

DOI: 10.1021/acs.langmuir.5b03291
Langmuir XXXX, XXX, XXX–XXX

organelles with different shapes. It also suggests that the local curvature of the membrane may play a crucial role.

■ ASSOCIATED CONTENT

Supporting Information

The Supporting Information is available free of charge on the ACS Publications website at DOI: 10.1021/acs.langmuir.5b03291.

SANS data of individual h- and d-NP, analytical derivation of lipid transfer kinetics models for bicelle and vesicle, SANS models to fit the bicelle and vesicle morphologies, detailed SANS fitting results, and comparison of three applied techniques (i.e., SANS, DSC, and FCS) (PDF)

■ AUTHOR INFORMATION

Corresponding Author

*E-mail: mu-ping.nieh@uconn.edu.

Notes

The authors declare no competing financial interest.

■ ACKNOWLEDGMENTS

The authors from UCONN would like to acknowledge the financial support from NSF-CMMI 1131587 and CBET 1433903. This work acknowledges additional support from the Scientific User Facilities Division of the US Department of Energy (DOE), Office of Basic Energy Sciences (BES), for use of the EQ-SANS instrument at the ORNL Spallation Neutron Source (SNS), which is managed by UT-Battelle, LLC, under Contract DE-AC05 00OR2275. J.K. is supported through the Scientific User Facilities Division of the DOE Office of Basic Energy Sciences (BES). The authors also wish to acknowledge the support received from Drs. C. Gao and W.T. Heller while conducting their experiments at the EQ-SANS facility. B.J. and Y.Z. also acknowledge the financial support from the US Department of Energy, Office of Basic Energy Science, Division of Materials Science and Engineering (DE-FG02-07ER46390).

■ REFERENCES

(1) Lev, S. Non-vesicular Lipid Transport by Lipid-Transfer Proteins and Beyond. *Nat. Rev. Mol. Cell Biol.* **2010**, *11*, 739−750.

(2) Maranhão, R. C.; Freitas, F. R. HDL Metabolism and Atheroprotection: Predictive Value of Lipid Transfers. *Adv. Clin. Chem.* **2014**, *65*, 1−41.

(3) Alpy, F.; Tomasetto, C. START Ships Lipids Across Interorganelle Space. *Biochimie* **2014**, *96*, 85−95.

(4) Neculai, D.; Schwake, M.; Ravichandran, M.; Zunke, F.; Collins, R. F.; Peters, J.; Neculai, M.; Plumb, J.; Loppnau, P.; Pizarro, J. C.; Seitova, A.; Trimble, W. S.; Saftig, P.; Grinstein, S.; Dhe-Paganon, S. Structure of LIMP-2 Provides Functional Insights With Implications for SR-BI and CD36. *Nature* **2013**, *504*, 172−176.

(5) Rashid, S.; Genest, J. Effect of Obesity on High-density Lipoprotein Metabolism. *Obesity* **2007**, *15*, 2875−2888.

(6) Balla, T. Phosphoinositides: Tiny Lipids with Giant Impact on Cell Regulation. *Physiol. Rev.* **2013**, *93*, 1019−137.

(7) Levine, T. Short-range Intracellular Trafficking of Small Molecules Across Endoplasmic Reticulum Junctions. *Trends Cell Biol.* **2004**, *14*, 483−90.

(8) Lebiedzinska, M.; Szabadkai, G.; Jones, A. W. E.; Duszynski, J.; Wieckowski, M. R. Interactions Between the Endoplasmic Reticulum, Mitochondria, Plasma Membrane and Other Subcellular Organelles. *Int. J. Biochem. Cell Biol.* **2009**, *41*, 1805−1816.

(9) Handa, T.; Saito, H.; Tanaka, I.; Kakee, A.; Tanaka, K.; Miyajima, K. Lateral Interactions of Pig Apolipoprotein-a-I with Egg-Yolk Phosphatidylcholine and with Cholesterol in Mixed Monolayers at the Triolein Saline Interface. *Biochemistry* **1992**, *31*, 1415−1420.

(10) Ram, P.; Prestegard, J. H. Magnetic Field Induced Ordering of Bile Salt/Phospholipid Micelles: New Media for NMR Structural Investigations. *Biochim. Biophys. Acta, Biomembr.* **1988**, *940*, 289−94.

(11) Sanders, C. R.; Hare, B. J.; Howard, K. P.; Prestegard, J. H. Magentically-oriented Phospholipid Micelles as a Tool for the Study of Membrane-associated Molecules. *Prog. Nucl. Magn. Reson. Spectrosc.* **1994**, *26*, 421−444.

(12) Kučerka, N.; Nieh, M.-P.; Katsaras, J. Fluid Phase Lipid Areas of Bilayers Thicknesses of Commonly Used Phophatidylcholines as a Function of Temperature. *Biochim. Biophys. Acta, Biomembr.* **2011**, *1808*, 2761−2771.

(13) Pan, J.; Cheng, X.; Monticelli, L.; Heberle, F. A.; Kučerka, N.; Tieleman, D. P.; Katsaras, J. The Molecular Structure of a Phosphatidylserine Bilayer Determined by Scattering and Molecular Dynamics Simulations. *Soft Matter* **2014**, *10*, 3716−25.

(14) Arriaga, L. R.; Lopez-Montero, I.; Monroy, F.; Orts-Gil, G.; Farago, B.; Hellweg, T. Stiffening Effect of Cholesterol on Disordered Lipid Phases: a Combined Neutron Spin Echo + Dynamic Light Scattering Analysis of the Bending Elasticity of Large Unilamellar Vesicles. *Biophys. J.* **2009**, *96*, 3629−3637.

(15) Heberle, F. A.; Petruzielo, R. S.; Pan, J.; Drazba, P.; Kučerka, N.; Standaert, R. F.; Feigenson, G. W.; Katsaras, J. Bilayer Thickness Mismatch Controls Domain Size in Model Membranes. *J. Am. Chem. Soc.* **2013**, *135*, 6853−9.

(16) Heberle, F. A.; Doktorova, M.; Goh, S. L.; Standaert, R. F.; Katsaras, J.; Feigenson, G. W. Hybrid and Nonhybrid Lipids Exert Common Effects on Membrane Raft Size and Morphology. *J. Am. Chem. Soc.* **2013**, *135*, 14932−5.

(17) Sanders, C. R.; Oxenoid, K. Customizing Model Membranes and Samples for NMR Spectroscopic Studies of Complex Membrane Proteins. *Biochim. Biophys. Acta, Biomembr.* **2000**, *1508*, 129−145.

(18) Marcotte, I.; Auger, M. Bicelles as Model Membranes for Solid- and Solution-state NMR Studies of Membrane Peptides and Proteins. *Concepts Magn. Reson., Part A* **2005**, *24A*, 17−37.

(19) Gregoriadis, G. Immunological Adjuvants: a Role for Liposomes. *Immunol. Today* **1990**, *11*, 89−97.

(20) Allen, T. M.; Cullis, P. R. Liposomal Drug Delivery Systems: from Concept to Clinical Applications. *Adv. Drug Delivery Rev.* **2013**, *65*, 36−48.

(21) Iqbal, U.; Albaghdadi, H.; Nieh, M.-P.; Tuor, U. I.; Mester, Z.; Stanimirovic, D.; Katsaras, J.; Abulrob, A. Small Unilamellar Vesicles: a Platform Technology for Molecular Imaging of Brain Tumors. *Nanotechnology* **2011**, *22*, 195102.

(22) He, H.-T.; Marguet, D. Detecting Nanodomains in Living Cell Membrane by Fluorescence Correlation Spectroscopy. *Annu. Rev. Phys. Chem.* **2011**, *62*, 417−436.

(23) Rigler, R.; Mets, Ü.; Widengren, J.; Kask, P. Fluorescence Correlation Spectroscopy with High Count Rate and Low Background: Analysis of Translational Diffusion. *Eur. Biophys. J.* **1993**, *22*, 169−175.

(24) Nakano, M.; Fukuda, M.; Kudo, T.; Endo, H.; Handa, T. Determination of Interbilayer and Transbilayer Lipid Transfers by Time-resolved Small-angle Neutron Scattering. *Phys. Rev. Lett.* **2007**, *98*, 238101.

(25) Lu, J.; Bates, F. S.; Lodge, T. P. Chain Exchange in Binary Copolymers Micelles at Equilibrium: Confirmation of the Independent Chain Hypothesis. *ACS Macro Lett.* **2013**, *2*, 451−455.

(26) Nakano, M.; Fukuda, M.; Kudo, T.; Miyazaki, M.; Wada, Y.; Matsuzaki, N.; Endo, H.; Handa, T. Static and Dynamic Properties of Phospholipid Bilayer Nanodiscs. *J. Am. Chem. Soc.* **2009**, *131*, 8308−8312.

(27) Choi, S.-H.; Bates, F. S.; Lodge, T. P. Molecular Excahnge in Ordered Diblock Copolymer Micelles. *Macromolecules* **2011**, *44*, 3594−3604.

(28) Lu, J.; Choi, S.-H.; Bates, F. S.; Lodge, T. P. Molecular Exchange in Diblock Copolymer Micelles: Bimodal Distribution in Core-Block Molecular Weights. *ACS Macro Lett.* **2012**, *1*, 982−985.

DOI: 10.1021/acs.langmuir.5b03291
Langmuir XXXX, XXX, XXX−XXX

(29) Klump, H. H.; Gaber, B. P.; Peticolas, W. L.; Yager, P. Thermodynamic Properties of Mixtures of Deuterated and Undeuterated Dipalmitoyl Phosphatidylcholines (Differential Scanning Calorimetry Lipid-Bilayers Membranes). *Thermochim. Acta* **1981**, *48*, 361−366.
(30) Bayerl, T. M.; Schmidt, C. F.; Sackmann, E. Kinetics of Symmetric and Asymmetric Phospholipid Transfer between Small Sonicated Vesicles Studied by High-sensitivity Differential Scanning Calorimetry, NMR, Electron Microscopy, and Dynamic Light Scattering. *Biochemistry* **1988**, *27*, 6078−6085.
(31) Reinl, H. M.; Bayerl, T. M. Lipid Transfer between Small Unilamellar Vesicles and Single Bilayers on a Solid Support: Self-assembly of Supported Bilayers with Asymmetric Lipid Distribution. *Biochemistry* **1994**, *33*, 14091−14099.
(32) Drazenovic, J.; Ahmed, S.; Tuzinkiewicz, N. M.; Wunder, S. L. Lipid Exchange and Transfer on Nanoparticle Supported Lipid Bilayers: Effect of Defects, Ionic Strength, and Size. *Langmuir* **2015**, *31*, 721−31.
(33) Hu, A.; Fan, T.-H.; Katsaras, J.; Xia, Y.; Li, M.; Nieh, M.-P. Lipid-based Nanodiscs as Models for Studying Mesoscale Coalescence − a Transport Limited Case. *Soft Matter* **2014**, *10*, 5055−5060.
(34) Liu, Y.; Li, M.; Yang, Y. K.; Xia, Y.; Nieh, M.-P. The Effects of Temperature, Salinity, Concentration and PEGylated Lipid on the Spontaneous Nanostructures of Bicellar Mixtures. *Biochim. Biophys. Acta, Biomembr.* **2014**, *1838*, 1871−1880.
(35) Nieh, M.-P.; Harroun, T. A.; Raghunathan, V. A.; Glinka, C. J.; Katsaras, J. Spontaneously Formed Monodisperse Biomimetic Unilamellar Vesicles: The Effect of Charge, Dilution and Time. *Biophys. J.* **2004**, *86*, 2615−2629.
(36) Nieh, M.-P.; Dolinar, P.; Kučerka, N.; Kline, S. R.; Debeer-Schmitt, L. M.; Littrell, K. C.; Katsaras, J. Formation of Kinetically Trapped Nanoscopic Unilamellar Vesicles from Metastable Nanodiscs. *Langmuir* **2011**, *27*, 14308−16.
(37) Jing, B.; Zhu, Y. Disruption of Supported Lipid Bilayers by Semihydrophobic Nanoparticles. *J. Am. Chem. Soc.* **2011**, *133*, 10983−10989.
(38) Petrášek, Z.; Schwille, P. Precise Measurement of Diffusion Coefficients using Scanning Fluorescence Correlation Spectroscopy. *Biophys. J.* **2008**, *94*, 1437−1448.
(39) Losonczi, J. A.; Prestegard, J. H. Improved Dilute Bicelle Solutions for High-resolution NMR of Biological Macromolecules. *J. Biomol. NMR* **1998**, *12*, 447−451.
(40) Benoit, H.; Picot, C.; Benmouna, M. Structure Factor of a Polymer in a Complex System by Small-Angle Neutron-Scattering. *J. Polym. Sci., Polym. Phys. Ed.* **1984**, *22*, 1545−1548.
(41) Guinier, A.; Fournet, G. *Small-Angle Scattering of X-rays*; Wiley: New York, 1955; p 268.
(42) Tristram-Nagle, S.; Liu, Y.; Legleiter, J.; Nagle, J. F. Structure of Gel Phase DMPC Determined by X-ray Diffraction. *Biophys. J.* **2002**, *83*, 3324−3335.
(43) Nagle, J. F.; Wiener, M. C. Structure of Fully Hydrated Bilayer Dispersions. *Biochim. Biophys. Acta, Biomembr.* **1988**, *942*, 1−10.
(44) Nieh, M. -P; Glinka, C. J.; Krueger, S.; et al. SANS Study of the Structural Phases of Magnetically Alignable Lanthanide-Doped Phospholipid Mixtures. *Langmuir* **2001**, *17*, 2629−2638.
(45) Struck, D. K.; Pagano, R. E. Insertion of Fluorescent Phospholipids into the Plasma Membrane of a Mamalian Cell. *J. Biol. Chem.* **1980**, *255*, 5404−5410.
(46) Wimley, W. C.; Thompson, T. E. Exchange and Flip-Flop of Dimyristoyl Phosphatidylcholine in Liquid-Crystalline, Gel and Two-Component, Two Phase Large Unilamellar Vesicles. *Biochemistry* **1990**, *29*, 1296−1303.
(47) Wimley, W. C.; Thompson, T. E. Transbilayer and Interbilayer Phospholipid Exchange in Dimyristoylphosphatidylcholine/Dimyristoylphosphatidylethanolamine Large Unilamellar Vesicles. *Biochemistry* **1991**, *30*, 1702−1709.
(48) Kleinfeld, A. M.; Chu, P.; Romero, C. Transport of Long-Chain Native Fatty Acids across Lipid Bilayer Membranes Indicates That Transbilayer Flip-Flop is Rate Limiting. *Biochemistry* **1997**, *36*, 14146−14158.
(49) John, K.; Schreiber, S.; Kubelt, J.; Herrmann, A.; Müller, P. Transbilayer Movement of Phospholipids at the Main Phase Transition of Lipid Membranes: Implications for Rapid Flip-Flop in Biological Membranes. *Biophys. J.* **2002**, *83*, 3315−3323.
(50) Ferrell, J. E.; Lee, K.-J.; Huestis, W. H. Lipid Transfer between Phosphatidylcholine Vesicles and Human Erythrocytes: Exponential Decrease in Rate with Increasing Acyl Chain Length. *Biochemistry* **1985**, *24*, 2857.
(51) Pownall, H. J.; Hickson, L.; Smith, L. C. Transport of Biological Lipopiles: Effect of Lipophile Structure. *J. Am. Chem. Soc.* **1983**, *105*, 2440.
(52) Nichols, J. W. Thermodynamics and Kinetics of Phospholipid Monomer-Vesicle Interaction. *Biochemistry* **1985**, *24* (23), 6390−8.
(53) Tanford, C. *The Hydrophobic Effect: Formation of Micelles and Biological Membranes*; Wiley: New York, 1973; p viii.
(54) Marsh, D. Thermodynamics of Phospholipid Self-assembly. *Biophys. J.* **2012**, *102*, 1079−87.
(55) Marsh, D. *Handbook of Lipid Bilayers*, 2nd ed.; CRC Press, Taylor & Francis Group: Boca Raton, FL, 2013; p *xxvii*.
(56) duPlessis, J.; Ramachandran, C.; Weiner, N.; Muller, D. G. The Influence of Lipid Composition and Lamellarity of Liposomes on the Physical Stability of Liposomes upon Storage. *Int. J. Pharm.* **1996**, *127*, 273−278.
(57) Devaux, P. F.; Fellmann, P.; Hervé, P. Investigation on Lipid Asymmetry Using Lipid Probes - Comparison between Spin-Labeled Lipids and Fluorescent Lipids. *Chem. Phys. Lipids* **2002**, *116*, 115−134.
(58) Israelachvili, J. N.; Marcelja, S.; Horn, R. G. Physical Principles of Membrane Organization. *Q. Rev. Biophys.* **1980**, *13*, 121−200.
(59) Jencks, W. P. *Catalysis in Chemistry and Enzymology*; Dover: New York, 1987; p xvi.
(60) Rowe, B. A.; Neal, S. L. Fluorescence Probe Study of Bicelle Structure as a Function of Temperature: Developing a Practical Bicelle Structure Model. *Langmuir* **2003**, *19*, 2039−2048.

DOI: 10.1021/acs.langmuir.5b03291
Langmuir XXXX, XXX, XXX−XXX